MORPHOLOGICAL STUDY OF KOSHI RIVER AT CHATARA AND ITS INFLUENCE ON INTAKE OF SUNSARI MORANG IRRIGATION PROJECT, NEPAL

Mahesh Maharjan[*]
MEE 19716

Supervisors: Dr. Daisuke Harada[**]
Dr. Atsuhiro Yorozuya[***]
Prof. Shinji Egashira[****]
Prof. Fukui Hideo[*****]

ABSTRACT

The study aimed to understand the formation of bars and their behaviors, which can change the morphology of the Koshi River at Chatara, where the Sunsari Morang Irrigation Project (SMIP) was constructed to withdraw water from the river to feed the irrigation canal. Every year, substantial amounts of sediment are deposited near the intake area, interrupting sufficient water flow towards the intake during the dry season. The depth-integrated two-dimensional (2D) numerical model was used for the analysis. The study indicated the formation of a mid-channel bar, which could not be eliminated by constricting the river width downstream, whereas the location of the mid-channel bar changed when adding a spur upstream. These forced bars were formed due to the river bend upstream of the channel. In the presence of a mid-channel bar, there is not sufficient flow of water towards the intake in the dry season, whereas enough water could be diverted towards the intake with the addition of the spur.

Keywords: river morphology, 2D flow simulation, bed deformation, flow pattern, sediment transport rate

INTRODUCTION

The Koshi Basin has a wide range of geographic variations and is prone to hazards such as floods, landslides, and debris flows. The basin has a drainage area of approximately 58,000 km^2 at Chatara. The Koshi River (Class I river) is the largest river in Nepal and one of the most dynamic rivers in the world, originating from the Himalayas in Tibet and flows towards the south plains of Nepal to meet the Ganges River in India. The rapid change in the gradient of river from the Himalayas to the lowland area causes heavy downstream sedimentation obtained from the young, fragile mountains. The study area lies where the river widens from a confined area. An abundant amount of sediment is deposited annually at Chatara, which has affected the intake of the Sunsari Morang Irrigation Project (SMIP). The project has been struggling to withdraw the required discharge of water from the river during the dry season due to sedimentation. This study helps to understand the flow patterns, sediment transport characteristics, and riverbed variations of the river. Therefore, different cases were simulated for the study, including the constriction of the river width downstream and consideration of a spur along the right bank upstream of the intake of SMIP. The depth-integrated two-dimensional (2D) flow simulation model was employed to analyze the bed deformations and flow patterns.

[*] Engineer, Department of Water Resources and Irrigation (DWRI), Nepal
[**] Associate professor, GRIPS, Tokyo and Research specialist, ICHARM, Tsukuba, Japan
[***] Associate professor, GRIPS, Tokyo and Senior Researcher, ICHARM, Tsukuba, Japan
[****] Professor, GRIPS, Tokyo and Research and Training Advisor, ICHARM, Tsukuba, Japan
[*****] Professor, GRIPS, Tokyo

METHODOLOGY

The depth-integrated 2D governing equations employed for the study consist of the mass and momentum conservation equations of water flow and the mass conservation equations of suspended sediment and bed sediment. The mass conservation equation for water flow in the Cartesian coordinate system is described as follows:

$$\frac{\partial \mathrm{h}}{\partial \mathrm{t}} + \frac{\partial}{\partial \mathrm{x}}(\mathrm{uh}) + \frac{\partial}{\partial \mathrm{y}}(\mathrm{vh}) = 0 \tag{1}$$

The *x* component of the momentum conservation equation for water flow is described as

$$\frac{\partial uh}{\partial t} + \frac{\partial uuh}{\partial x} + \frac{\partial uvh}{\partial y} = -gh\frac{\partial}{\partial x}(h + Z_b) - \frac{\tau_x}{\rho} + \frac{\partial}{\partial x}(h\sigma_{xx}) + \frac{\partial}{\partial y}\left(h\tau_{yx}\right) \tag{2}$$

The *y* component of the momentum conservation equation for water flow is described as

$$\frac{\partial vh}{\partial t} + \frac{\partial vuh}{\partial x} + \frac{\partial vvh}{\partial y} = -gh\frac{\partial}{\partial y}(h + Z_b) - \frac{\tau_y}{\rho} + \frac{\partial}{\partial x}\left(h\tau_{xy}\right) + \frac{\partial}{\partial y}\left(h\sigma_{yy}\right) \tag{3}$$

where, h = flow depth, t = time, u and v are the depth-averaged flow velocity in the x and y directions, respectively, g is the acceleration due to gravity, Z_b is the bed elevation, ρ is the mass density of water, σ_{xx}, σ_{yy}, τ_{xy}, and τ_{yx} are the Reynolds stresses, and τ_x and τ_y are the components of bed shear stress (τ_b) in the x and y directions, respectively.

The mass conservation equation for the suspended sediment is described as follows:

$$\frac{\partial c_i h}{\partial t} + \frac{\partial r_1 u c_i h}{\partial x} + \frac{\partial r_1 v c_i h}{\partial y} = \frac{\partial}{\partial x}\left(h\varepsilon_x \frac{\partial c_i}{\partial x}\right) + \frac{\partial}{\partial y}\left(h\varepsilon_y \frac{\partial c_i}{\partial y}\right) + E_i - D_i \tag{4}$$

where, c_i is the depth-averaged value for the sediment concentration, ε_x and ε_y are the x and y components of the dispersion coefficient, r_1 is the correction factor, and E_i and D_i are the erosion and deposition rates of the suspended sediment for grain size d_i, respectively.

The mass conservation equation of the bed sediment is described as follows:

$$\frac{\partial Z_b}{\partial t} + \frac{1}{1-\lambda}\sum_i \left(\frac{\partial q_{bix}}{\partial x} + \frac{\partial q_{biy}}{\partial y} + E_i - D_i\right) = 0 \tag{5}$$

where, Z_b is bed elevation, E_i and D_i are the erosion and deposition rates of the suspended sediment for grain size d_i, $\mathrm{q_{bi}}$ is the bed load transport rate for grain size d_i, and λ is the porosity of bed sediment.

The bed load transport equation by Egashira et al. (1997b, 2005) was employed, which is described as:

$$q_{b*} = \frac{4}{15}\frac{K_1 K_2}{\sqrt{f_d + f_f}}\tau_*^{\frac{5}{2}} \tag{6}$$

where, q_{b*} is the non-dimensional bed load transport rate, τ_* is the non-dimensional bed shear stress, and K_1, K_2, f_d, and f_f are specified theoretically.

The erosion rate was evaluated using Itakura and Kishi's formula (1980), which is described as:

$$\frac{E}{u_*} = K\frac{\omega_0}{u_*}\left(\alpha_* \frac{\sigma - \rho}{\sigma}\frac{gd}{u_*\omega_0}\Omega - 1\right) \tag{7}$$

$$\Omega = \frac{\tau_*}{B_*}\frac{\int_{a'}^{\infty} \xi \frac{1}{\pi}\exp(-\xi^{2)} d\xi}{\int_{a'}^{\infty} \frac{1}{\pi}\exp(-\xi^{2)} d\xi} + \frac{\tau_*}{B_*\eta_0} - 1$$

$$a' = \frac{B_*}{\tau_*} - \frac{1}{\eta_0}$$

where, E is the erosion rate, w_o is the settling velocity of a sediment particle, K, α_*, B_*, and η_0 are empirical coefficients, u_* is the shear velocity, τ_* is the non-dimensional bed shear stress.

Figure 1 shows the study methodology. Based on the governing equations described above, the depth-integrated 2D simulation model iRIC-Nays2DH developed by Yasuyuki SHIMIZU and Hiroshi TAKEBAYASHI, 2014, was employed with modifications mentioned above. The river discharge, river slope, and sediment particle size were set as inputs in the model. The initial, boundary, and other computational conditions were also set up. The bed deformations were simulated to understand the temporal and spatial changes in the riverbed elevation. In addition, simulations for flow patterns were also conducted with low flow discharge.

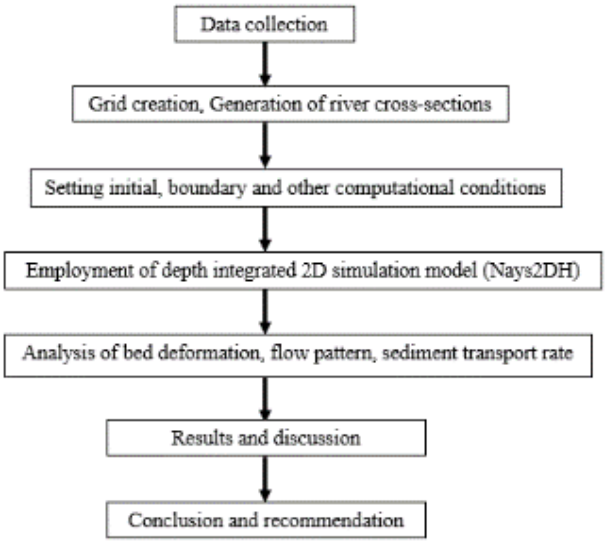

Figure 1: Framework of Methodology

DATA

As the bathymetry data of the river was not available, a flat river channel bed was used as the initial river topography. The left bank and right bank alignments of the study domain were created by obtaining the location of the bank from satellite images. The steady flood discharge of Q = 8,000 m^3/s, which was calculated as the average annual maximum flood discharge at the Chatara gauge station from 1977 to 2015, was established as the upstream boundary condition. Figure 2 shows the sediment particle size distribution assumed by the field situation, which was set as the initial condition for the entire study reach. Manning's roughness coefficient = 0.04, channel bed slope = 0.005, and calculation time step = 0.2 s were given.

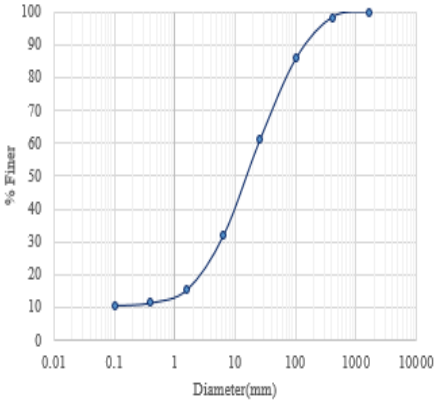

Figure 2: Sediment particle size distribution

RESULTS AND DISCUSSION

(1) Bed deformation analysis

Case A: Figure 3 shows the formation of bars (point bar and mid-channel bar) after simulating the flatbed topography for 120 days. The color contour values of the elevation change show erosion and deposition. The figure reveals that point bars were formed on the inside bend of the river, whereas a mid-channel bar, indicated by the blue ellipse, was formed in the middle of the channel. The mid-channel bar

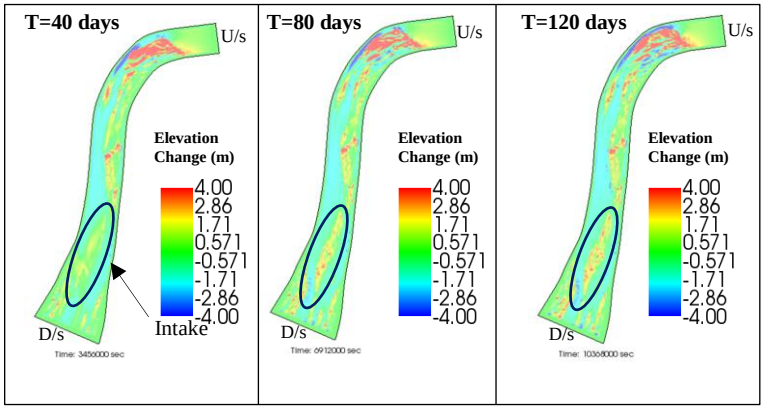

Figure 3: Temporal and spatial change in bed elevation (case A)

bifurcated the main channel into two sub-channels. The concentration of flow along the outer bend of the river increased the shear velocity, causing erosion. As the flow exited the bend, it dispersed owing to the channel widening downstream, which reduced the shear velocity and hence, deposition occurred, forming a forced bar. The figure also shows that the mid-channel bar was fixed in its position with no migration towards the right or left banks, as indicated in the 40, 80 and 120 d simulation results, interrupting sufficient water flow towards the intake during the dry season.

Case B: The mechanism for the formation of the mid-channel bar could have been due to the variation in river width when the river widened from a confined area. Therefore, in Case B, the river width downstream was reduced by 35% from the right bank to observe the effects on the mid-channel bar formation from the downstream constriction. The hatched triangular portion in Figure 4 shows the constricting obstacle with length = 1.5 km and width =350 m (35% of the river width downstream). The 120-d simulation result of bed deformation shows the formation of a mid-channel bar, as signified by the blue ellipse in the figure.

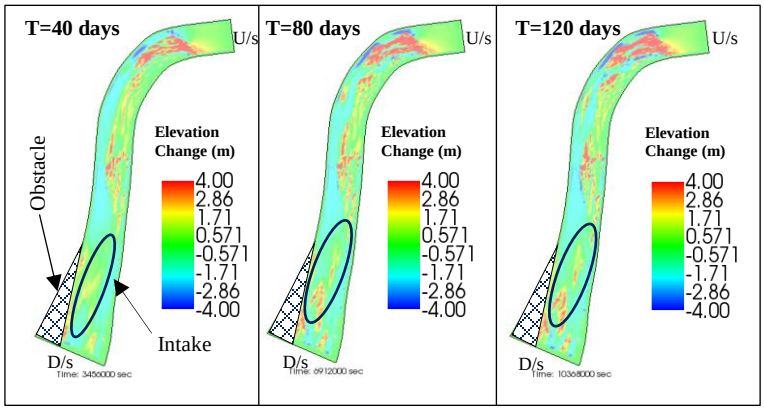

Figure 4: Temporal and spatial change in bed elevation (case B)

Case C: Since, the geometry of the mid-channel bar changed in Case B compared with Case A, which can be seen from the plan view, it was further necessary to investigate whether this bar would dissolve or shift to the left or right bank with a further decrease in the river width downstream. Therefore, Case C was considered in which the river width was reduced by 50% from the right bank. The hatched triangle in Figure 5 shows the obstacle of length = 1.5 km and width = 500 m (50% of the river width downstream). The 120-d simulation result of bed deformation also shows the presence of a mid-channel bar, indicated by the blue ellipse, in the same position as in the above cases. However, the geomety of this bar had changed.

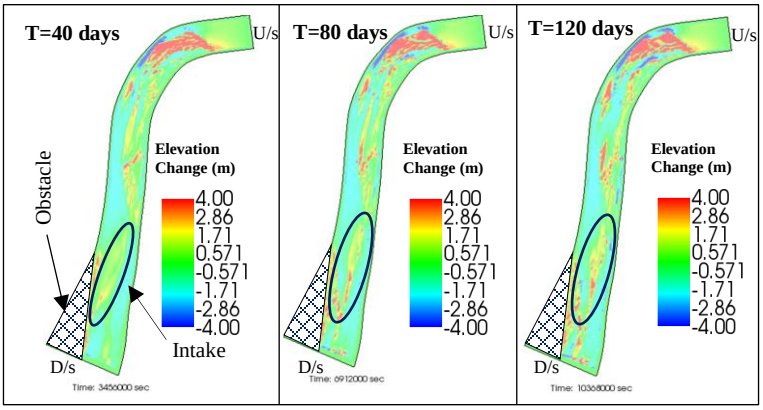

Figure 5: Temporal and spatial change in bed elevation (case C)

Case D: As, the observed mid-channel bar could neither be eliminated nor moved to the right bank by constricting

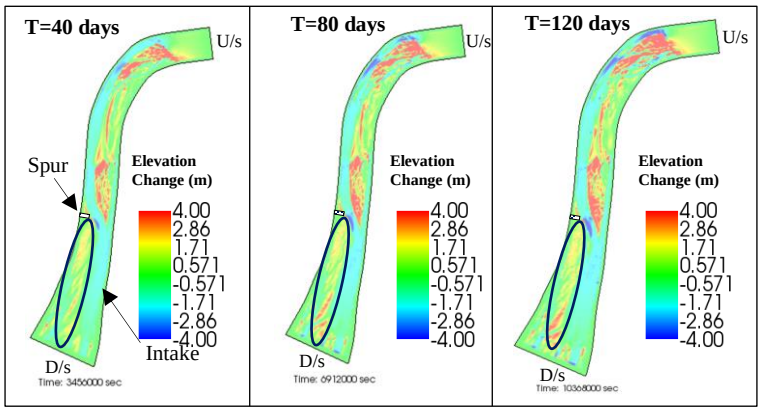

Figure 6: Temporal and spatial change in bed elevation (case D)

the river width downstream, the behavior of this bar under the provision of a spur along the right bank upstream was analyzed. Therefore, in Case D, a spur 750 m upstream of the intake in the right bank (the location where bifurcation started) was added to examine the effects of location of the mid-channel bar for the sufficient water diversion to the intake. The 120-d simulation of bed deformation shows the bar in the right bank (marked by the blue ellipse in Figure 6) instead of the mid-channel bar observed in the previous cases.

Case E: As, the mid-channel bar completely shifted to right bank in Case D, the flow would be concentrated along the left bank, which is suitable for the dry season, whereas, during the flood season, the area near the intake may have been affected. In order to further observe the changing behavior of the bar, Case E was considered in which the spur length of half that in case D was provided. The 120-d simulation result of bed deformation shows the formation of a bar (marked by a blue ellipse in Figure 7) that is different from Case D.

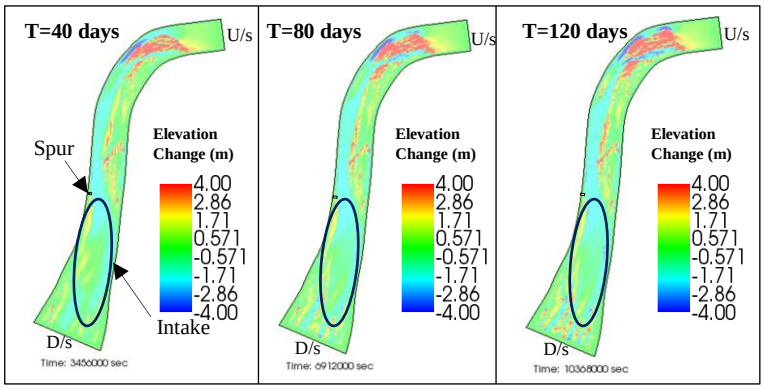

Figure 7: Temporal and spatial change in bed elevation (case E)

(2) Flow pattern analysis

Since, there was a problem of low water flow towards the intake during the dry season, it was necessary to analyze the flow pattern with dry flow discharge. Therefore, a 3-d flow simulation with a dry flow discharge of 200 m^3/s was conducted using the topography after 120 d of bed deformation for each case. Figure 8 shows the distribution of flow in the right and left channels. The percentage of flow in the right channel was 95%, 98%, and 99% for Case A, Case B, and Case C, respectively. Thus, most of the water was flowing through the right channel, whereas minor flow occurred in the left channel. However, in Cases D and E, there was sufficient flow towards the left channel.

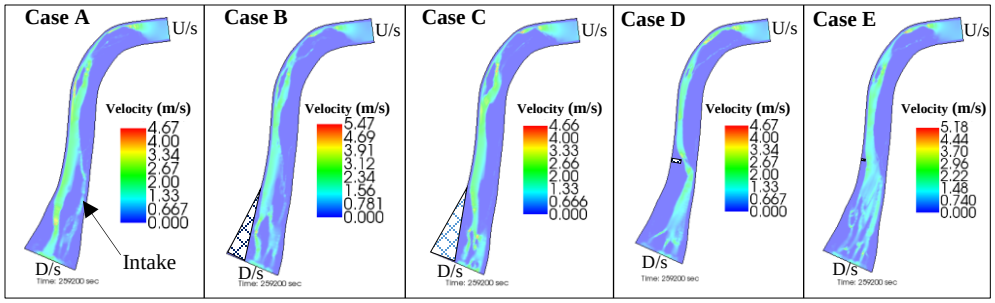

Figure 8: Distribution of flow

(3) Temporal change in sediment transport rate

Figure 9 shows the temporal change of bed load and suspended load transport rate at Section 1-1 (inflow section) and Section 2-2 (outflow section) for all cases. The inflow and outflow rates of sediment change with respect to time. At different points in time, the inflow rate of the bed load is larger than the outflow rate, whereas at other times, the outflow rate is larger. Therefore, both bed erosion and deposition take place within this section, creating an imbalance in the sediment budget. From the figure, it can be observed that

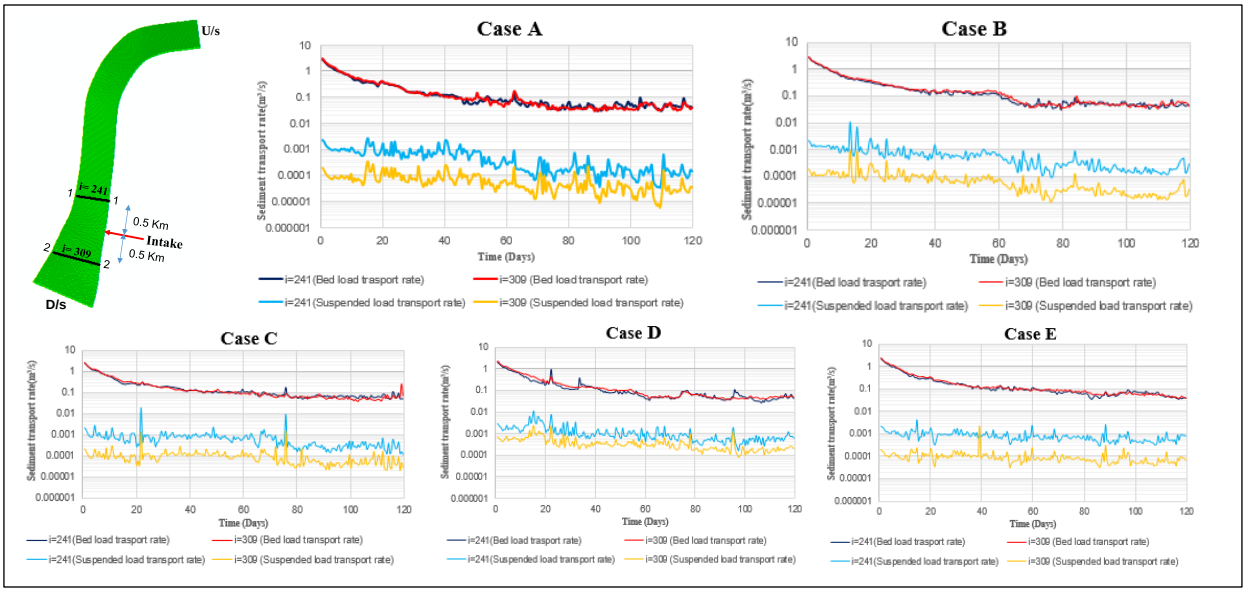

Figure 9: Temporal change of sediment transport rate

the bedload was dominant, with fine sediment also being deposited. However, the deposition of fine sediment in Case D seems to be less than that in other cases.

CONCLUSION AND RECOMMENDATION

The formation of bars and their behaviors were investigated by numerical simulation using a depth-integrated 2D model. The results revealed that the observed mid-channel bar could neither be eliminated nor be moved to the right bank by constricting the river width downstream. However, the provision of a spur changed the location of the mid-channel bar. These bars were forced bars that formed due to the river channel curvature in the upstream. With the mid-channel bar, there was not sufficient flow of water towards the intake during the dry season, whereas enough water could be diverted by adding a spur.

ACKNOWLEDGEMENT

I would like to express my sincere gratitude to my supervisors, Assoc. Prof. Daisuke Harada, Research Specialist, Assoc. Prof. Atsuhiro Yorozuya, Senior Researcher, Prof. Shinji Egashira, Research and Training Adviser, and ICHARM for their invaluable suggestions, support, and supervision during the course of the study.

REFERENCES

Egashira, S. 2009-2020. *Mechanics of Sediment Transportation and Channel Changes, Manual for Water-Related Risk Management Course*.

Jorge D. Abad and Marcelo H. Garcia, 2009. *Experiments in a High-Amplitude Kinoshita Meandering Channel: 2. Implications of Bend Orientation on Bed Morphodynamics*, Water Resources Research, 45, W02402, doi: 10.1029/2008WR007017.

Kafle MR, 2018. *Two-Dimensional Hydrodynamic Modelling of Koshi River and Prediction of Inundation Parameters*, Hydrology: Current Research, 9:2, doi: 10.4172/2157-7587.1000298.

Mat Salleh. M.Z, Ariffin. J, 2013. *Flow and Sediment Matrix in Mid-Channel Bar Formation*, International Journal of Scientific & Engineering Research, Volume 4, Issue 5, ISSN 2229-5518.

Shimizu,Y and Takebayashi, H, 2014. iRIC Software, *Changing River Science*, Nays2DH Solver Manual.